Astron. Astrophys. Suppl. Ser. 92, 333-348 (1992)

ASTRONOMY & ASTROPHYSICS
SUPPLEMENT SERIES

Astron. Astrophys. Suppl. Ser. **92,** 333-348 (1992)

The interstellar neutral-gas experiment on ULYSSES

M. Witte[1], H. Rosenbauer[1], E. Keppler[1], H. Fahr[2], P. Hemmerich[1], H. Lauche[1], A. Loidl[1] and R. Zwick[1]

[1] Max-Planck-Institut für Aeronomie, Katlenburg - Lindau, Germany
[2] Institut für Astrophysik der Universität Bonn, Germany

Received March 27; accepted September 20, 1991

Abstract. — The properties (density, bulk velocity relative to the solar system, and temperature) of the local interstellar gas, represented by neutral helium penetrating the heliosphere, will be measured *in-situ* for the first time by the ULYSSES GAS instrument. By employing the solar gravitational field as a natural velocity analyser, the bulk velocity relative to the solar system and the temperature of the gas can be derived from the angular distributions of the particles measured in at least two widely separated points in the heliosphere. The gas density can be determined if a composition corresponding to cosmic abundances is assumed. The neutral particles are detected via the secondary electrons or ions which are emitted upon particle impact from a freshly deposited lithium-fluoride (LiF) layer. The physical principles and assumptions on which the experiment is based, the main technical features of the instrument, and first measurements in space are briefly described.

Key words: space instruments — interstellar medium — UV radiation.

1. Scientific objectives.

A sizeable fraction of the mass of galaxies is not condensed in stars but rather distributed in interstellar space as atoms or molecules: the interstellar gas. This matter is not only of interest as a remnant of extinguished stars and the building material of new ones, it is also the medium in which cosmic-ray particles propagate and get accelerated to high energies. Most general, it is a (still unknown) mixture of neutral and ionized components. As our solar system moves through this matter with a relative velocity of about 20 km/s, the solar wind and its intrinsic magnetic field form a bubble (the heliosphere) which cannot be penetrated by the interstellar plasma but is transparent to the neutral component. To understand the complex interactions between the heliospheric and the interstellar components taking place in the transition region a detailed knowledge also of the distribution and the state of the interstellar medium is required. (For an overview the reader may be referred to recent reviews by Cox & Reynolds 1987; Holzer 1989 and references therein, and to a series of most recent papers in Grzedzielski & Page 1990.)

Important information about the distant interstellar medium outside the heliosphere has been achieved from radio observations and measurements of interstellar absorption lines towards nearby stars (e.g. Lallement *et al.* 1990). Inside the heliosphere the neutral component can be taken as a representative of the local interstellar matter. The spatial distribution of the most prominent constituents, hydrogen and helium, have most extensively been investigated in the past using UV scattering methods (Bertaux & Blamont 1971; Weller & Meier 1974; Chassefière *et al.* 1986; for a review see e.g. Holzer 1989). These techniques suggested that the temperatures of H and He are different by about a factor of 2. Also the densities of H and He derived from these measurements seemed to indicate an abundance ratio different from cosmic abundances. This discrepancy can be resolved by assuming a red-shift in the solar He lines (Chassefière *et al.* 1988). Also the direct measurement of interstellar pick-up ions, developed very recently (Möbius *et al.* 1985; 1988), led to a He temperature $T_{He} = 7000 - 12500$K which would be consistent with the now widely accepted value of the H temperature $T_H \approx 8000$K.

In the evaluation of the optical measurements some assumptions have to be made about the profiles and intensities of solar UV lines and about the ionization rate of the neutral particles leading to a significant scatter in the results of different measurements and a still sizeable uncertainty in the values of density, velocity and temperature.

More accurate results, at least on the kinetic parameters, can be gained if the velocity distribution of the particles penetrating the solar system is determined directly.

Send offprint requests to: M. Witte.

However, this has hitherto not yet been accomplished. Even though the flux of neutral interstellar atoms near the Earth's orbit is $> 10^4$ cm^{-2}s^{-1}, neutral particles have not been detected because of the problems the measurement poses. Usually, neutral particles to be measured are ionized first, and then their energy and direction is determined by common energy per charge or mass per charge analysers. However, because of the particles' high velocity, the ionization probability in an electron-collision ionization source is only of the order of 10^{-5} to 10^{-6}. Therefore, this method has never been tried.

2. The measuring principle of the instrument.

Because of the above mentioned difficulties, a new approach is undertaken now for the first time with the GAS instrument. Use is made of the fact that the neutral helium particles penetrating the solar system are hardly affected by light pressure and charge exchange and therefore essentially follow Keplerian orbits (hyperbolae). It can be shown that knowledge of the angular flux distribution of helium in only two points of the solar system is, in principle, sufficient for deriving velocity, temperature, and density of the local interstellar helium. This means in practice that the measurements should be made in two widely separated points, where the orbital planes of the particles are not co-planar with respect to the symmetry axis of the flow field.

This measurement principle is demonstrated in Figure 1. For simplicity, it is first assumed that the thermal velocity of the particles at large distances from the Sun is negligible. Then, an observer would measure a parallel beam of particles anywhere in the solar system (except on the symmetry axis). If in point A of Figure 1 the flow direction a (unit vector) of the particles is determined, their orbital plane is known since it must contain the center of the Sun. If a corresponding measurement is made in a different plane in point B, the symmetry axis of the flow velocity field and thus the flow direction of the particles at "infinity" is known. Since the orbits of the particles are hyperbolic and their asymptotic direction of arrival must be parallel to the symmetry axis, the speed "at infinity" of the particles can be determined from either of the two measurements. Thus, the density of the interstellar helium and its flow velocity relative to the solar system can be determined from the measured directions and fluxes.

This principle works also if the temperature of the gas outside the solar system is non-zero. Then, even though the procedure is significantly more complicated as also the spacecraft's orbital velocity must be taken into account (Rosenbauer *et al.* 1987), the distribution function can still be reconstituted from measurements of angular distributions at the points A and B (Banaszkiewicz *et al.* 1990).

With the above scheme the measurement problem is reduced to that of finding a suitable detector for the neutral particles under consideration. Then, in addition only a mechanical collimator placed in front of the detector and a space probe with a scanning platform providing access to suitable measurement positions are required.

3. Instrument description.

3.1. THE DETECTION MECHANISM.

If, as in this experiment, the main goal is the in-situ measurement of the neutral helium, both secondary electron and ion emission are suitable detection mechanisms.

The problem with secondary electron emission as a detection mechanism is that photoelectrons can seriously disturb the measurement, and secondary ion emission usually has the disadvantage of a rather small yield. However, during development of this experiment one material, namely lithium-fluoride (LiF), was found that exhibits little of these disadvantages with respect to both detection processes (Rosenbauer & Fahr 1977). Since LiF is transparent to UV-light, Ly-α photons, which are the most disturbing source of background, have a low photoelectron yield, provided the surface is clean. As LiF is an ionic crystal, the efficiency for secondary ion production is comparatively high, since most of the sputtered atoms leave the surface ionized. When bombarded with neutral helium atoms, the yield Li^+ is much higher than that of F^- because of the better momentum transfer from He to Li.

When, subsequently, the Li^+-ions are accelerated by an electric field to a particle detector, at the same time photoelectrons are suppressed. Therefore, a detector system based on the release of Li^+ from a LiF surface can be made very insensitive to UV photons. They can contribute to the count rates only by generating positive ions (a very unlikely process) or when they are scattered somehow into the particle detector.

Efficiencies for secondary electron and ion production from helium atoms have been determined by Raphelt (1982), and those measured later by Bleszynski (1985) with a set-up identical to the flight unit of the GAS-experiment are shown in Figure 2. Both processes are strongly energy dependent. At energies around 80 eV both efficiencies are of the same order of about 10^{-2}, towards lower energies the efficiencies fall off rapidly. Therefore, an instrument based on LiF as a conversion surface is only useful for neutral helium detection if the particle energy is above $\sim$ 30 eV, corresponding to $\sim$ 27 km/s. This is the case for the first half year after the launch of ULYSSES, when the velocities of the spacecraft and the particles add favorably, and also in extended period around perihelion.

Due to the rapid fall-off of the efficiency with decreasing particle energy, which also holds for particles other

than helium, a detector of the kind described here is essentially blind to interstellar hydrogen. It should be very sensitive to heavier particles, but their fluxes are expected to be so small that most of the detected signals will be due to neutral helium. However, it may be possible to detect, and separate, fluxes of heavier particles, like oxygen, due to their expected narrower angular distribution. Secondary electrons as well as ions can easily be counted after post-acceleration by conventional particle detectors, such as Channel Electron Multipliers (CEMs).

3.2. THE INSTRUMENT'S SENSOR HEAD.

Schematic cross-sections of the sensor head are shown in Figure 3, and details of the subunits in Figure 4. Two nearly identical detector channels are housed in a vacuum-tight box of $9.1 \times 5.6 \times 3.4$ cm. The fields of view are limited by two circular apertures each to full opening angles of 4.9° in channel (I) and 7.4° for channel (II). The outer apertures (9, 11) are protected by a simple, asymmetric baffle (13) against direct sunlight. During ground operations and launch the sensor was sealed by releasable, vacuum-tight covers (7). Incoming particles first pass electrostatic deflection systems, which serve as filters against charged particles up to energies per charge of $\approx$ 80 kV in channel (I) and $\approx$ 50 kV in channel (II) due to a DC-voltage between the plates. The conversion plates consisting of reduced (black and conductive) lead glass are mounted on ceramic thick-film resistors, used as heaters to bake out the conversion plates at temperatures up to 200°C. The plates, with an effective area of about 8×10 mm, are inclined by 45° to the optical axis towards the channeltrons (4) and by 28° towards the furnace (3). By heating the furnace mounted in the middle between the two channels, LiF is evaporated and deposited simultaneously on both the conversion plates and a small quartz crystal (2) used to monitor the thickness of the deposited layers (see Sect. 3.3.).

Secondary particles released from the conversion plates are accelerated towards the funnel of the CEMs (4) (one for each channel) by an electric field between the conversion plate and the plane grid (transmissivity 80%) in front of the CEM. The acceleration potential is derived from the high-voltages for the channeltrons (see Fig. 5), which can be selected by telecommands. It is about -2700 V (84% of the negative high-voltage) for detection of the positive secondary ions or about $+420$ V (16% of the positive high-voltage) for detection of secondary electrons.

The CEMs (4) are special, custom-made devices in blocks of ceramic material with an aperture of 5×5 mm, minimizing the surfaces sensitive to penetrating cosmic radiation and, in particular, to γ–rays from the spacecraft Radio Thermal Generator (RTG). Tiny tungsten filaments (6) which can be heated by telecommand are used to stimulate the CEMs during ground testing in vacuum, providing an end-to-end test of the whole instrument.

The hybrid thick-film pulse amplifiers, discriminators and shapers (5), the inflight test pulse generator and the quartz-oscillator circuits are mounted inside the vacuum-tight housing. For all non-metallic items inside the sensor box (e.g. circuit boards, insulators etc.) ceramic material is used to avoid potential contamination of the CEMs from (organic) outgassing products.

The two channels (I) and (II) are always operated simultaneously in the same mode (electron or ion detection). Their fields of view are defined by circular apertures (see Fig. 3: apertures 9, 10, 11, 12 have 3.5, 3.4, 7.0, 3.4 mm diameter, respectively) separated by 81 mm, resulting in full opening angles of 4.9° (7.4°), respectively. For isotropic fluxes the geometric factor is 0.13×10^{-3} (0.53×10^{-3}) cm^2 sr, respectively; for point sources the effective area is at maximum 9.08 mm^2 and depends on boresight angle α from the optical axis of the detector system as indicated in Figure 6. The fact that the channels are different only with respect to their fields of view eases the determination of background.

The sensor head is mounted on a turntable which forms an integral part of the instrument. The rotation axis of the turntable is oriented perpendicular to the spin axis of the spacecraft. This way the "elevation" angle between the spin axis and the optical axis of the sensor can be varied between 0° and 180° with a minimum step width of 1°. Then, together with the rotation of the spacecraft, the whole celestial sphere can be scanned (see Fig.11).

3.3. THE LiF EVAPORATION SYSTEM.

One of the essential subunits in this experiment is the device to evaporate layers of fresh LiF on the conversion plates. It has to fulfill several, non-standard constraints, which shall be described here in more detail:

1. The LiF must be kept chemically clean as its transparency to UV-light and its efficiency of secondary ion production depends on its purity. However, in hot or even molten state LiF is chemically very aggressive. Also, it is slightly hygroscopic, therefore it must be kept in an inert, dry nitrogen-atmosphere throughout handling and/or storage.
2. As there was less than 2 W of heating power available, a sophisticated design with a minimum of heat losses was required.
3. In order to get as many as possible, new, sufficiently thick ($\sim$ 8 nm) layers from the limited amount of LiF in the supply, it is mandatory to strictly adjust and control the evaporation rate.

To achieve these requirements, the following design was realized:

Figure 7 shows the tiny furnace, filled with about 2 mm^3 of LiF. It consists of a helix (1 mm diameter,

3 mm length) of platinum wire (0.1 mm diameter and a total resistance of $\sim 0.7\Omega$ at ambient temperature). On telecommand this helix heats the LiF efficiently up to about 600°C, where a mild evaporation of the LiF starts.

A quartz crystal, mounted at the same distance from the furnace as the conversion plates, is used to monitor the thickness of the evaporated layers. Its resonance frequency (2.09 MHz) drops with the thickness of the evaporated LiF layer with $\Delta f = 21$ Hz/nm. By comparing the frequency with a reference frequency from the spacecraft clock, the frequency variations are measured and telemetered with 1 Hz resolution in housekeeping parameter VF.

Plans to use this monitor to directly control the evaporation process and to stop the evaporation as soon as a desired thickness is achieved, had to be discarded, because of the too large temperature dependence of the quartz being directly exposed to the hot furnace and the complexity of the required electronics circuits. The approach chosen is shown in Figure 8. The temperature of the furnace is measured by the increase in the resistance of its platinum helix ($\sim 2\Omega$ at 600°C), which is used in the bridge circuit to control the electrical power provided to the oscillator. The power, required to get the desired evaporation rate, can easily be adjusted with the bridge circuit. According to the time selected by telecommand, the evaporation process is stopped automatically after 2.5 or 5.0 minutes. These two times allow to cope with variations in the evaporation rate due to different filling states of the furnace.

The supply is sufficient for a total thickness of 150 nm of the deposited layers, i.e. for about 20 evaporation processes. To get the full detection efficiency a thickness of about 10 nm is required for the first layer, further "refreshing" layers may be thinner.

3.4. TECHNICAL DESCRIPTION.

3.4.1. *History.*

Originally, the GAS-experiment had been selected for the payload of the NASA spacecraft. It consisted of the neutral helium instrument (Rosenbauer & Fahr 1977) and two absorption cells for H Ly-α and He 58.4 nm observations, included later, to be provided by French groups. When, in 1981, NASA cancelled its spacecraft it was decided - in view of the difficulties involved - to include the neutral particle instrument in the payload of the ESA spacecraft: as the design of the ESA spacecraft at that time was already frozen-in and the engineering model was about ready for testing, severe constraints had to be met by the new GAS-instrument, some of which were: minimal mass and power allocations (1.6 kg, 0.7 W), no changes to the electrical spacecraft interface (harness, commanding, telemetry), only minimal changes to the mechanical interface, and an engineering model had to be delivered in time for the start of the spacecraft testing. This allowed only about 3 months to almost completely redesign the instrument according to the new constraints and to manufacture an engineering model. Thanks to the cooperation of the PI of the EPAC-instrument (E. Keppler) who permitted to use part of his telemetry and command capacity, and to the almost super-human effort of up to 14 skilled and dedicated individuals in the Max-Planck-Institut during the design and manufacturing phase of the instrument, and thanks to the kind support of many other persons in various institutions, it was possible to salvage the GAS-experiment for the ESA-ULYSSES-spacecraft.

Several of the features in the instrument, described in the following paragraph, are simply a result of these circumstances (and will not be discussed further).

3.4.2. *Mechanical design features.*

The turntable, or "stepping platform", is an indispensable subsystem of the instrument as scanning of a nearly 4π solid angle is necessary. Operation of this platform by telecommands must be safe and accurate (accuracy better than $\pm 0.2°$), but high scanning velocity is not required.

For the bearing the following concept was adopted. All axial loads are carried by an axial ball bearing supporting the whole circumference (150 mm diameter) of the turntable and the radial loads are taken over by a central bolt. In the circumferential ball bearing an aluminium disk is suspended between two rings of Delrin balls such that a large differential radial expansion of the rotating and the fixed parts of the bearing can be tolerated. For the central (radial) bearing a 3 mm titanium bolt/polyimide washer combination was chosen to exclude the possibility of cold welding under vacuum. For the same reason the two-step gear was made in part of glass-fibre-enforced polyimide. A modified commercial stepper motor (56 steps per revolution) was chosen as the active element. All parts except the gear and the axles were machined from aluminium alloy (AlMgSi1).

The turntable is an integral part of the electronics box and essentially replaces its front wall (Fig. 9). To give the box both high accuracy and low weight, a design employing a milled aluminium frame with glued-on walls of 0.2 mm thick aluminium was adopted. Due to the semi-cylindrical shape, a high stiffness at low weight could be achieved. The cylindrical mantle consists of a 0.3 mm aluminium sheet, which is strapped across the box and serves the double purpose of stiffening the box and holding the plug-in electronics boards in place. The mass budget of the instrument is summarized in Table 1.

3.4.3. *Survey of the instrument electronics.*

A block diagram of the instrument electronics, also indicating the locations of the subsystems in the instrument, is shown in Figure 5. The instrument's two entrance lids are kept closed by means of a solder joint. This joint can

be broken by a heater which is initiated by applying 28 V to the cover-release line.

Depending upon whether the neutral particles are to be detected via their secondary-electron or secondary-ion emission, either the positive or the negative CEM high-voltage power supply is switched on by telecommand. Both DC/DC converters employ an oscillator (tuned to 80 kHz) on the primary and a five-stage Cockcroft-Walton generator on the secondary side. Feedback from the first stage ensures sufficiently high stability. Both supplies can be commanded to a first level of 2200 V, then the voltage can be increased in seven steps of 150 V each. The potentials for the CEM funnels and the charged-particle filters are also derived from the CEM high-voltage supplies.

The CEM pulse amplifiers are thick-film hybrids mounted close to the CEMs in the vacuum-tight sensor compartment. To achieve noise immunity and suppress false pulses generated by ionizing radiation penetrating the CEMs, a comparatively high threshold of 2×10^6 e is chosen. The thresholds can be checked by initiating a chain of simulated CEM pulses with decreasing amplitude from a test-pulse generator (Sect. 4).

Electrical connection to the turntable is made by means of a flexible "printed circuit". To avoid the need for flexible high-voltage lines, all high-voltage converters are mounted on the rotating part of the instrument.

Analogue to digital converters on the basis of voltage-controlled oscillators provide digital housekeeping data of 16 analogue values.

The digital electronics is based on available radiation-hard parts of the RCA 4000 series. The only exceptions are the memories used for data storage. Here, two radiation-hard TC 244s are employed in ping-pong mode. The digital system receives, decodes, and verifies four different command words and controls the state of the experiment and the performance of the measurements according to their contents. A summary of the power consumption during various operational modes is given in Table 2.

3.5. Data-channel summary.

The science data consist of 64 (16-bit) words (A00...A31, B00...B31) containing the counts of the two channeltrons (A and B) accumulated during one GAS measurement cycle (GMC) in 32 spin related, azimuth-sectors. The housekeeping data (64 bytes) providing command verification, digital and digitized analogue housekeeping values are summarized in Table 3. The relative timing of these data and their occurrence in the data stream are shown in Figure 10. With the occurrence of a 2^3−FMT-pulse one experiment data cycle (EDC) is started, which lasts 34 minutes and consists of 8 experiment data frames (EDF).

All the data are routed through one multiplexer (Fig. 5: DS2 MUX) into the data stream of the EPAC-instrument (compare Fig. 5 in Keppler *et al.*, this volume); when after switch-on of the instrument, this multiplexer is enabled by a special telecommand, the syncword in FRM 0, FMT 0 is set to 161_8, verifying that GAS-data are transmitted.

Altogether 200 bytes per two EDCs are allocated to the GAS-instrument, which means a bit rate of 0.4 bit/s at a spacecraft telemetry rate of 1024 bit/s. At this rate a total operation time of 102 minutes is required to get one complete GAS-data cycle (2 EDCs for accumulation + 1 EDC for transmission).

3.6. Instrument commanding and operation.

3.6.1. *General.*

A list of the GAS commands is given in Table 4. The four command words are shared with the EPAC-instrument, however, the GAS commands can be identified by the bits 15, fixed to 1, and bits 6 fixed to 0, also bits 14 and 6 have to be inverse to each other. Each of the four command words is dedicated to a special purpose, indicated in the headline of Table 4. We concentrate here on those command capabilities controlling the performance of the scientific measurements (mainly contained in commands 1 and 3).

During those periods of the mission when the particles have a sufficiently high velocity relative to the spacecraft to exceed the required energy threshold the particle flow is always highly supersonic. This means that its angular spread is small, of the order of a few degrees FWHM. The angle of approach varies widely during the mission. Therefore, a high flexibility in the scanning programmes is required.

In the GAS coordinate system, defined in Figure 11, an area of "interest" can be specified by the maximum and minimum angles both in elevation and in azimuth. These parameters as well as the resolution in elevation can be selected rather freely and sent to the instrument to perform the required scanning programme.

3.6.2. *Azimuthal scanning.*

For the azimuthal scanning the spacecraft spin is employed. An azimuthal scan can be started at a look angle α_0, where α_0 can be any multiple of 11.25° in the range 0°-348.75°. Then the instrument measures over 32 adjacent bins (segments) with the width α_n, which can be chosen from the values 0.7°, 1.4°, 2.8° or 11.25°. This way azimuthal ranges of 22.5°, 45°, 90° or 360° can be resolved. During the subsequent rotations of the spacecraft the measurements are repeated in the same segments and the counts measured are added up and stored in 32 dedicated registers for each of the two detector channels. This is normally continued for the duration of two EDCs (68 min at the spacecraft tracking data rate of 1024 bit/s). For special purposes, shorter integration periods lasting only a few (1-127) spacecraft revolutions can also be com-

manded. With the beginning of the next odd EDC the stepping platform normally moves to the next elevation value, however, it can be commanded to stay at this position for n measurement cycles, with $n = 1...7$.

3.6.3. *Scanning in elevation.*

For scanning in elevation the instrument stepping platform is employed. Similar to the azimuthal scanning the start value for a scan in elevation ε_0 (so-called "south fan edge") can be chosen from any multiple of 16° in the range $0° - 176°$. From this position the platform can move to m further positions in increments of $\Delta\varepsilon$ (step width), performing in each position the azimuthal measurements as described in section 3.6.2. With the available values for m ($m = 0,2,4 \ldots 28, 30$) and $\Delta\varepsilon$ ($\Delta\varepsilon = 1°, 2°, 4°, 8°$) a large variety of ranges in elevation between ε_0 and $(\varepsilon_0 - m \cdot \Delta\varepsilon)$ can be scanned with the resolution $\Delta\varepsilon$. After m steps have been performed, the platform automatically reverses its direction, thus continuously scanning between the extreme positions until further instructions are received by telecommand.

4. Testing and calibration.

End-to-end tests of the instrument have been performed, using a PC-based ground support equipment (GSE). The GSE served as a spacecraft simulator, providing all spacecraft-generated signals, as well as a data receiving and evaluation system which picked the GAS data out of the spacecraft data stream and displayed the data in predefined formats.

With the sensor head being evacuated, the overall-performance of the fully integrated instrument could be checked by stimulating the channeltrons with the built-in filaments or by externally applied γ-ray sources. The performance of the channeltrons was verified checking their high-voltage characteristic by commanding the 8 high-voltage levels.

Without the sensor head being evacuated, a near end-to-end test was performed by means of the inflight test generator (see Sect. 3.4.2.) feeding simulated CEM-pulses into the test input of the CEM-amplifier, which were counted in every fourth EDC in the azimuthal sector $\alpha_0 = 0$.

The 16 analogue housekeeping values included in the science data stream provide nearly exhaustive information on the health of the instrument since potentials and currents on all important supply lines and the temperature of the sensor head are monitored regularly. The conversion from the 8-bit telemetry counts into physical values is summarized in Table 5. For a complete check-out of the data memories, a special command is foreseen: all-ones or all-zeros can be read into the memory.

As the information about the velocity and the temperature of the interstellar neutral helium is contained in the position and in the width of the measured distribution in inertial space, special effort was put into the calibration of the position of the stepping platform.

The position information is available from two independent housekeeping parameters providing redundancy and cross-check. In the "analogue"-platform position, the reading of a high-precision linear potentiometer, digitized in 12 bit, is available with a resolution of 0.12°. The "digital"-platform position provides the contents of an up/down counter summarizing the number of steps of the stepper motor. The regression curves ε_A and ε_D (Tab. 5) for the absolute platform position are derived from simultaneous measurements of the actual position in absolute angles and the "digital"- and "analogue" housekeeping values. A one-σ deviation of 0.4° includes the play of the gear as well as thermal drifts in the analogue measurement.

Both parameters are normalized in the instrument's frame of reference by moving the platform to the mechanical end-stop in the "north"-position ($\varepsilon = 0$) (here actually the up/down counter is set to zero). This normalization can be enforced at any time by telecommand.

In space, an additional possibility exists for checking the correct performance of a solid angle scan. Since the instrument is sensitive to UV light with wavelengths below 110 nm bright UV stars can be detected. The star map that can be derived from the data allows cross-checking and accurate calibration of the angular housekeeping data.

An absolute calibration of the detection efficiency of the instrument is difficult. Measurements by Bleszynski (1985) (see Fig. 2) indicate the uncertainties due to systematic errors and aging of the LiF layer which has been observed in laboratory tests and may be due to e.g. potential contamination from the environment or migration of impurities in the layer. However, in flight the cleanliness of the LiF layer on the conversion plate can be checked in several ways. First, on a regular basis, by comparing the response of the instrument to both neutral particles and UV light immediately before and after a fresh layer had been deposited. Second, the instrument's response to a UV star can be monitored by choosing a suitable scanning programme. A degradation of the LiF surface should result in an increased response of the instrument to UV light. If this is observed, a fresh LiF layer will be deposited.

5. Inflight performance and first results.

The instrument was initially switched on 14 days after the successful launch of the ULYSSES-spacecraft on October 6, 1990. The following weeks were dedicated to check-out and configuration of the instrument: the sensor covers were opened, the proper operation and angular calibration

of the stepping platform was verified. After several days to allow for outgassing of the sensor housing the performance of the CEMs was proven by applying the various high-voltage levels.

During the first three months of operation about 250 telecommands were sent to the instrument to perform all the check-out-, configuration- and measurement programmes. The mechanical turntable worked absolutely flawless in the measured temperature range between +18°C and −28°C, and also, all other operations were performed to full satisfaction.

With five evaporation processes a LiF layer of about 11 nm thickness was achieved. The rate of evaporation was smaller than expected as the flight unit of the LiF furnace has slightly different characteristics than the one used to adjust the control loop in the heating electronics (Sect. 3.3). However, this provided an additional opportunity to observe the built-up of the secondary ion response with the increasing thickness as well as the reduction of the UV-background in the electron mode. Within the first two months after switch-on no evidence was found that the performance of the deposited LiF layers degraded. However, further depositions of fresh layers have been scheduled to check the long-term stability of the performance.

One of the first measurements in the secondary ion mode with the final LiF layer is shown in Figure 12. A cartesian representation of the spherical coordinate system (Fig. 11) of the instrument is used to plot the count rates as a function of the viewing direction. In this coarse survey one pixel corresponds to a resolution of 11.25° in azimuth and 8° in elevation.

At the time of this measurement (day 335, 1990) the spacecraft was very close to the symmetry axis (see Fig.1) of the neutral gas flow downstream of the Sun in the area of the neutral gas enhancement due to gravitational focussing. At a given point of the symmetry axis the arrival directions of the particles form a cone centered around this axis. From all these particles those are detected with highest efficiency which are moving in the ecliptic plane ($\alpha = 270°$), because their velocity adds with the spacecraft velocity to the highest relative energy in the spacecraft system. Particles arriving from directions inclined to the ecliptic plane have less relative energy and are therefore detected less efficiently. This gives rise to the "banana"-shaped distribution centered at $\alpha \approx 270°$, $\varepsilon = 80°$ in Figure 12, the first in-situ observation of interstellar neutral helium in space.

Spots of one or two pixels result from single or several UV stars as has been verified later in measurements with high-angular resolution.

At small offset angles from the Sun, sunlight illuminates the inner part of the baffle and is more easily scattered into the detector resulting in the high count rates around $\alpha \approx 220°$, $\varepsilon \approx 150°$. Closer to the Sun the high voltage of the channeltrons is switched off the save their lifetimes.

As the omnidirectional background resulting from penetrating cosmic rays, the RTG-radiation, or from "dark-counts" (about 0.4 counts/s) is less than expected, a very useful signal to background ratio of about 10 is achieved.

From measurements like in Figure 12 and from many further measurements, performed later with better angular resolution ($\Delta\varepsilon = 2°$), it will be possible to determine the location and the width of the angular distribution in inertial space with sufficient precision to achieve the goal of determining the parameters (velocity, temperature and density) of the interstellar neutral gas.

Acknowledgements.

We are deeply indebted to numerous persons who contributed to the development of this experiment and to even more who supported us during the rescue action. K.-P. Wenzel, ULYSSES Project Scientist, did his best to keep this experiment alive; the ESA Project Team (D. Eaton, W. Frank, P. Caseley, H. Schaap, G. Tomaschek), and the Dornier System Spacecraft Team, represented by R. Nord and D. Kolbe, showed their understanding and gave valuable support in spite of the additional work load that the late implementation of the instrument caused for them.

Design, construction and testing of an essentially new instrument in the extremely short time available would not have been possible without the enthusiasm, dedication, endurance and skill of many co-workers at the MPI für Aeronomie, W. Barke, W. Boogaerts, H.G. Engelmann, K. Fischer, B. Gräve, M. Krause, G. Schlemm, U. Spilker, U. Strohmeyer, K.H. Thiele, G. Umlauft, the members of the workshop. They and many others who could not be mentioned here have contributed to solving a problem that had once appeared nearly insoluble.

Financial support to the GAS project was provided by the Bundesminister für Forschung und Technologie through the DFVLR-PT/DARA (010N28 WRK275 and 500N87052).

References

Banaszkiewicz M., Rosenbauer H., Witte M. 1990, Proc. lst COSPAR Colloq. on Physics of the Outer Heliosphere, Warsaw 1989, Eds. S. Grzedzielski, D.E. Page, (Pergamon Press) 359

Bertaux J.L., Blamont J.E. 1971, A&A 11, 200

Bleszynski S. 1985, Measurements of secondary ion, electron and photon yields of Pb-glass and LiF surfaces upon impact of He-atoms in the energy range of 23 to 3000 eV. Internal Report MPAE-T-77-85-26, Max-Planck-Institut für Aeronomie, Katlenburg-Lindau, FRG

Chassefière E., Bertaux J.L., Lallement R., Kurt V.G. 1986, A&A 160, 229

Chassefière E., Dalaudier F., Bertaux J.L. 1988, A&A 201, 113

Cox D.P., Reynolds R.J. 1987, ARA&A 25, 303

Holzer T.E. 1989, ARA&A 27, 199

Grzedzielski S., Page D.E. Eds. 1990, Proc. lst COSPAR Colloq. on Physics of the Outer Heliosphere, Warsaw 1989 (Pergamon Press) 409 p

Lallement R., Ferlet R., Vidal-Madjar A., Gry C. 1990, Proc. lst COSPAR Colloq. on Physics of the Outer Heliosphere, Warsaw 1989, Eds. S. Grzedzielski, D.E. Page (Pergamon Press) 37

Möbius E., Hovestadt D., Klecker B., Scholer M., Gloeckler G., Ipavich F.M. 1985, Nature 318, 426

Möbius E., Klecker B., Hovestadt D., Scholer M. 1988, Ap&SS 144, 487

Raphelt M. 1982, Untersuchungen zur Möglichkeit des Nachweises von interstellarem Neutralgas im interplanetaren Raum mit Hilfe der Sekundärionenemission,
PhD. thesis, Univ. Göttingen, FRG

Rosenbauer H., Witte M., Pietsch J.F., Fahr H.J., Lay G. 1987, Proc. Int. Workshop on Problems of Physics of Neutral Particles in the Solar System, Zakopane / Poland 1985, Universität Bonn and Max-Planck-Institut für Aeronomie, Katlenburg-Lindau, FRG, 139

Rosenbauer H., Fahr H.J. 1977, Direct measurement of the fluid parameters of the nearby interstellar gas using helium as tracer. Experiment Proposal for the Out-of-Ecliptic Mission, Internal Report, Max-Planck-Institut für Aeronomie, Katlenburg-Lindau, FRG

Weller C.S., Meier R.R. 1974, ApJ 193, 471

TABLE 1. *Mass summary.*

Subsystem	Mass (g)
Platform, incl. motor, gear and HV converters	395
Structure, incl. thermal interface	242
Analogue electronics board	52
Digital electronics, incl. power converter boards	472
Mother board, incl. interconnection harness to the EPAC instrument	229
Sensor head, incl. baffle and support ring for the local thermal blanket	182
Thermal blanket	25
Miscellaneous	31
Experiment total	1628

TABLE 2. *Power summary.*

Operation mode	Primary power (mW)
Experiment on (standby)	550
Normal operation	
High-voltage on	720–780[a]
Platform operation	780–840[a]
Special operations[b]	
Filament on	1490
LiF evaporation	2920[c]
Heater 1 or 2	1490
Cover release	1920

[a] Depending on the HV-level used
[b] Initiated by telecommand, for short periods
[c] After 40 seconds reduced to 1800 mW

TABLE 3. *The housekeeping information, read out in frame 1 of each telemetry format (FMT) of each odd experiment data cycle EDC (compare Fig. 10).*

	EDF 0	EDF 1	EDF 2	EDF 3	EDF 4	EDF 5	EDF 6	EDF 7	
FMT 0	ID 0	ID 1	ID 2	ID 3	ID 4	ID 5	ID 6	ID 7	EDF ID
1	VF	VF	VF	VF	VF	VF	VF	VF	Evaporation frequency
2	ELCC EL 1	EL 1	AZCC AZ 1	AZ 1	DACC DA 1	DA 1	HKCC HK 1	HK 1	Command verification
3	EL 2	EL 2	AZ 2	AZ 2	DA 2	DA 2	HK 2	HK 2	
4	PLPOS MSB	PLPOS MSB	DAFRM MSB	DAFRM MSB	L	L	SPINC MSB	SPINC MSB	Digital HK data
5	PLPOS LSB	PLPOS LSB	DAFRM LSB	DAFRM LSB	M	M	SPINC LSB	SPINC LSB	
6	PLTM MSB	I+28	I+6	I+HV	U+6	U+10	U+HV	TEMP	Analogue HK data
7	ICOV	I+10	I−10	I−HV	U+28	U−10	U−HV	PLTL LSB	

IDx = 00x fixed
DA 2, L, M = 000 fixed
MSB = Most Significant Byte
LSB = Least Significant Byte
PLPOS = Platform Position (digital)
DAFRM = Data Frame Counter
SPINC = Spin Counter
TEMP = Sensor temperature
PLTM = Platform Position (analogue)
PLTL
U_{xx}/I_{xx} = Voltage/current of xx supply line
ICOV = Current of heater for cover release

TABLE 4. *GAS schematic command list.*

Bit	COMMAND 1 Azimuth control	COMMAND 2 Data control	COMMAND 3 Elevation control	COMMAND 4 Housekeeping control
15	fixed 1	fixed 1	fixed 1	fixed 1
14	Start of azimuthal scan α_0 w.r.t. see–sun pulse ($\alpha = 0$)	GAS–data on/off	North movement	HV on/off
13		Command execution priority	South movement	HV level
12			Scan	
11			Elevation fan width m	
10		Measurement or memory test		HV polarity
9	Az. sector width			Heater 1 on/off
8				Heater 2 on/off
7	fixed 0	fixed 0	fixed 0	fixed 0
6				
5	Integration time		Elevation step width $\Delta\varepsilon$	Filament on/off
4				LiF evaporation
3		unused		
2	Platform control		Position south fan edge ε_0	Cover release
1				
0				az. contr. HV

TABLE 5. *Conversion of telemetered housekeeping values (Tab. 3) into physical values.*

HK–PARAMETER	UNIT	CONVERSION
Voltage (+ 6 V)	V	U = 0.035 · (U + 6)
Current (+ 6 V)	mA	I = 12.5 – 0.0785 · (I + 6)
Voltage (+ 10 V)	V	U = 0.066 · (U + 10)
Current (+ 10 V)	mA	I = 43.5 – 0.243 · (I + 10)
Voltage (+ 28 V)	V	U = 0.201 · (U + 28)
Current (+ 28 V)	mA	I = 47.27 – 0.305 · (I + 28)
Voltage (– 10 V)	V	U = –14.75 + 0.0706 · (U – 10)
Current (– 10 V)	mA	I = 0.0277 · (I – 10)
Voltage (+ HV)	kV	U = –0.67 + 0.0351 · (U + HV)
Current (+ HV)	mA	I = 0.073 · (I + HV)
Voltage (– HV)	kV	U = 0.0431 – 0.02764 · (U – HV)
Current (– HV)	mA	I = 0.15 + 0.068 · (I – HV)
Current (Cover)	mA	I = 0.275 · (I COV)
Sens. temperature	°C	T = 78.13 – 0.6565 · (TEMP)
Quartz–frequency	Hz	f = 1.1 · (VF)
Digital position	deg.	ε_D = 1.126 + 0.03128 · (PLPOS(M) + PLPOS(L))
Analogue position	deg.	ε_A = 335.273 + 0.1237 (16 · PLTM[a)] + PLTL[b)])

[a)] take PLTM from the next GAS–measurement cycle (GMC)
[b)] lowest four bits only

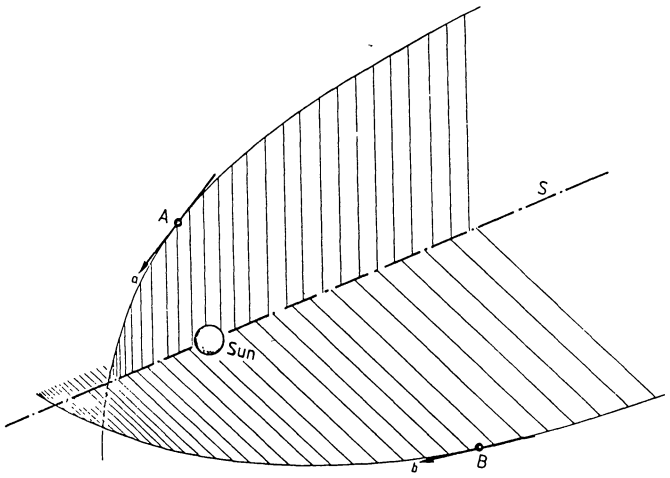

FIGURE 1. Use of the Sun's gravitational field for determining the velocity vector of a parallel beam of particles approaching from "infinity". If the particles' flow direction in two points (A, B) of the solar system has been determined, the flow direction at "infinity" is known since it must be parallel to the intersection S of the two orbital planes determined by the flow directions a and b and the center of the Sun. The speed at infinity can be derived either from angles between S and a or S and b and the coordinates of A and B, respectively.

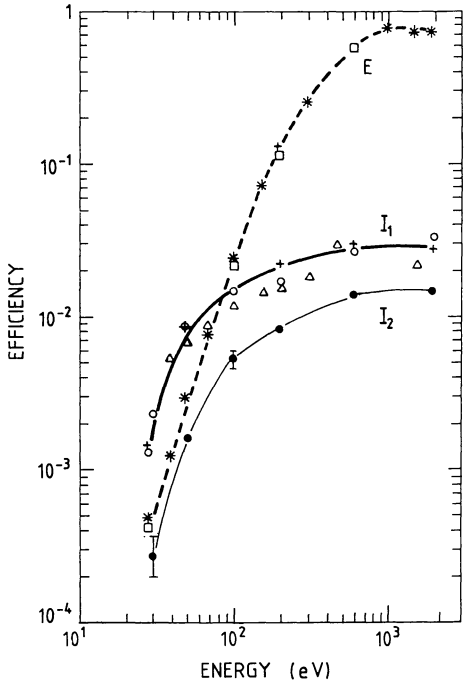

FIGURE 2. Efficiencies of the production of secondary electrons (E) and secondary ions (I_1) as a function of the energy of impacting helium atoms, measured at several times after deposition of the LiF layer. The values of curve I_1 are taken in vacuum, (+): 1 day after deposition of a 150 nm layer, (Δ): 6 days after deposition and, (o): 2 hours after deposition of a new, 50 nm layer, showing some scatter of up to 40% in the efficiency. Curve I_2, measured after the LiF layer had been exposed to air for about a month, shows that in the "worst" case of contamination the efficiency degrades only by about a factor of two. Values of curve E are measured ($\square$): 1 day and ($\star$): 6 days after deposition of a 150 nm layer.

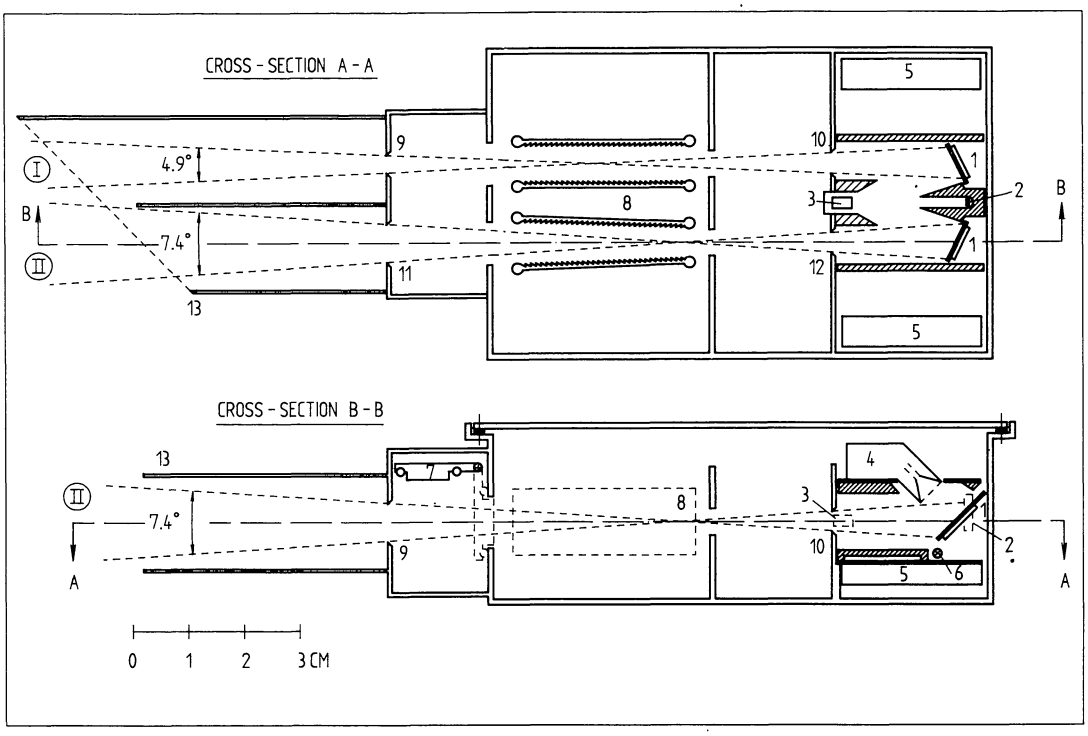

FIGURE 3. Cross-sections of the sensor head (schematic), 1) conversion plate with heater, evaporated with lithium-fluoride (LiF), 2) quartz crystal for monitoring the LiF evaporation process, 3) furnace with LiF supply, 4) channel electron multiplier (CEM), 5) CEM-amplifier and electronics (s. Fig. 5), 6) tungsten-filaments to stimulate the CEMs, 7) vacuum-tight cover in closed (dashed lines) and open position, 8) electrostatic deflection system to filter out charged particles, 9, 10) circular apertures defining the field of view of channel (I), 11, 12) circular apertures defining the field of view of channel (II), 13) light baffle.

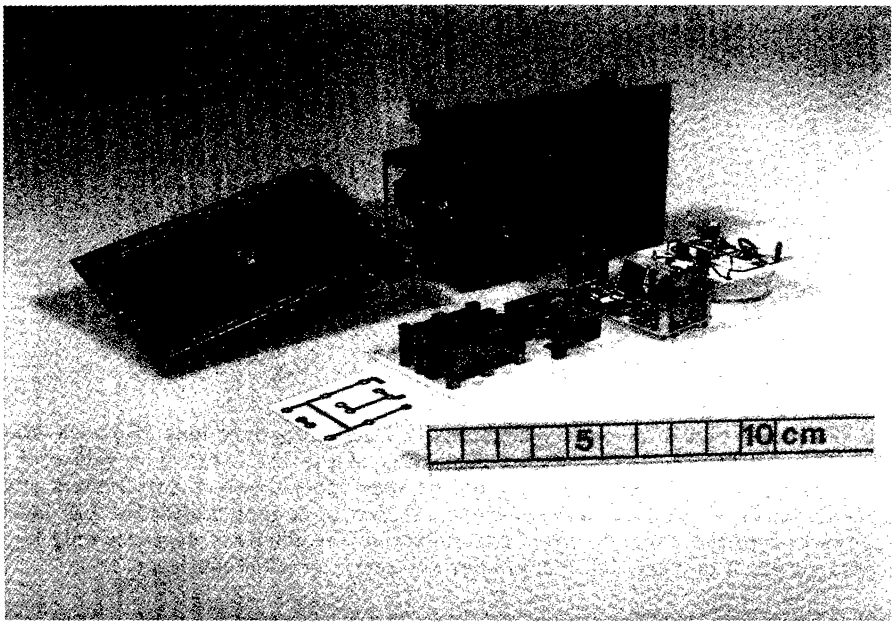

FIGURE 4. The subunits of the sensor head (see also Fig. 3), from left: the electrostatic deflection system; support structure; lower electronics board with the black conversion plates and the CEM-amplifiers standing up at the outer edges; the upper electronics board with the high-voltage connections for the CEMs.

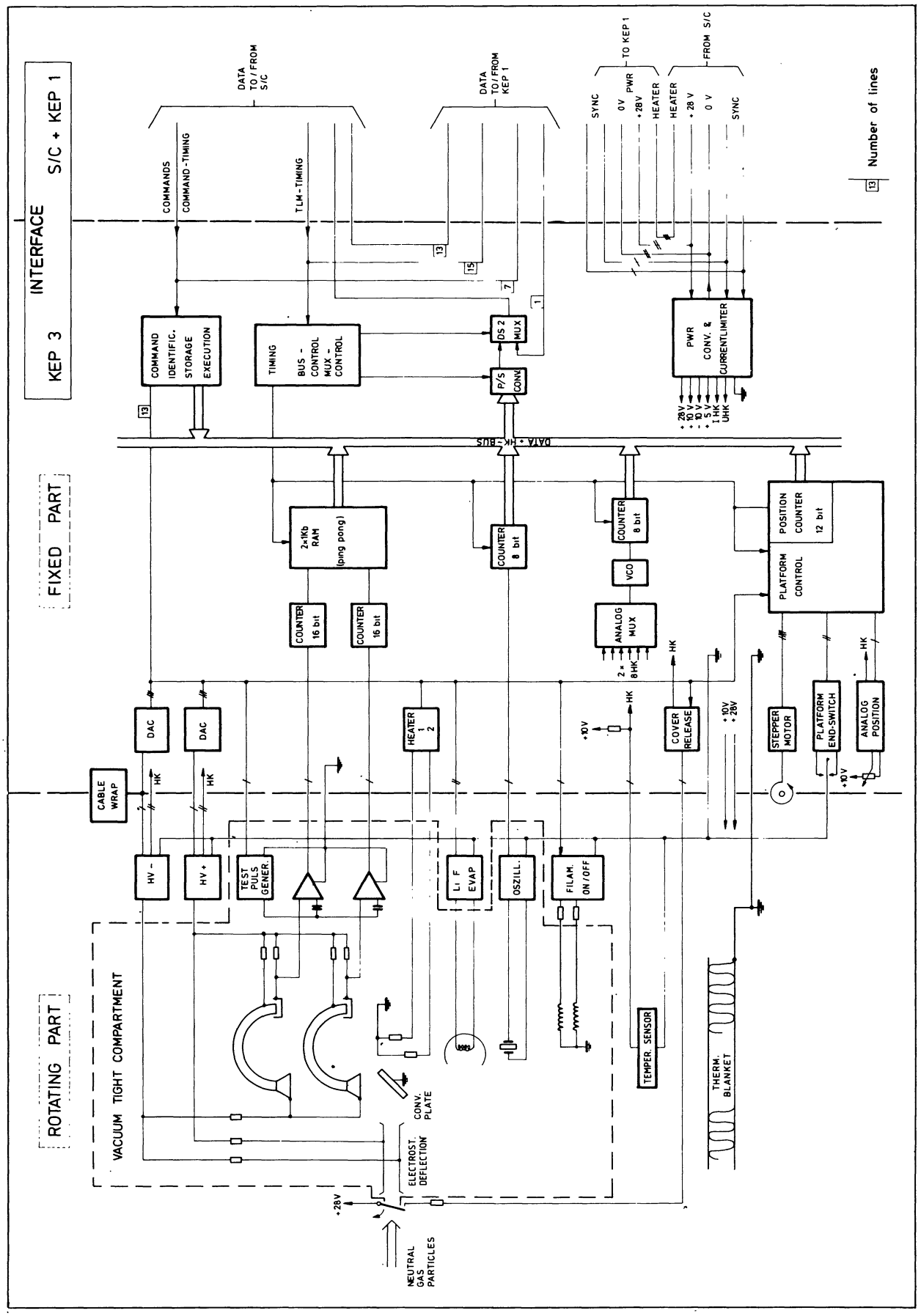

FIGURE 5. Block diagram of the instrument electronics, also indicating the locations of the sub-systems.

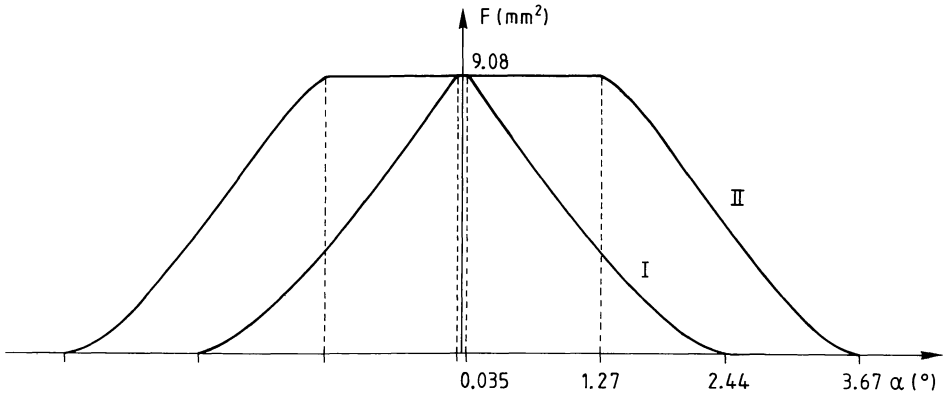

FIGURE 6. Effective active area of systems (I) and (II) for a point source with a boresight angle α to the optical axis of the systems.

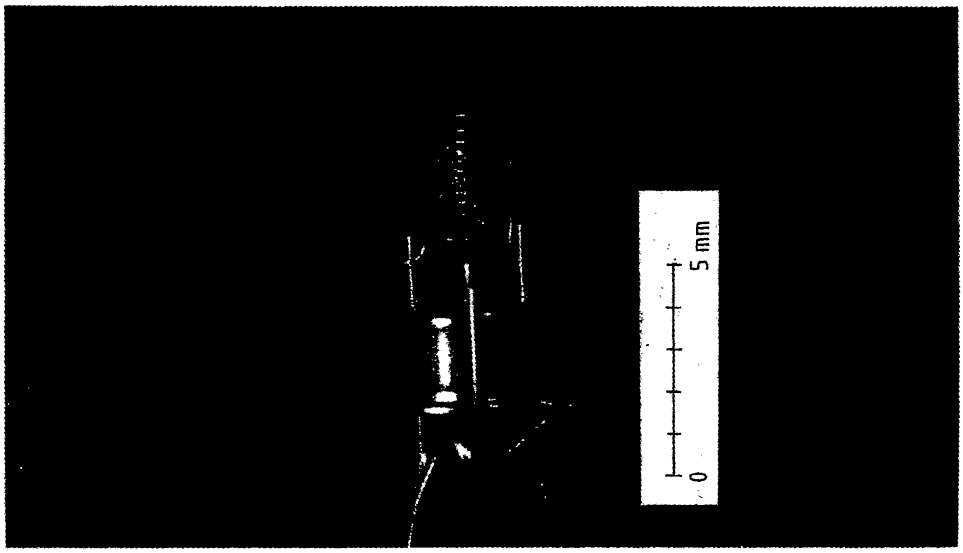

FIGURE 7. The LiF furnace, with the outer housing removed. The helix contains about 2 mm^3 of molten LiF.

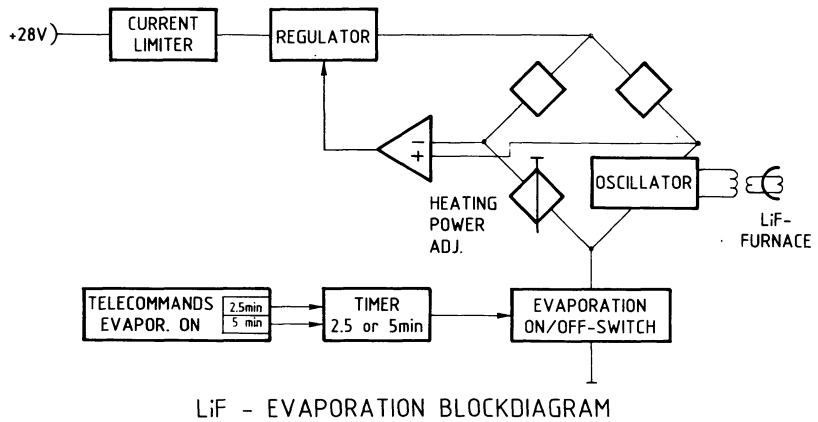

FIGURE 8. Block diagram of the electronics to heat up the LiF furnace to a regulated temperature.

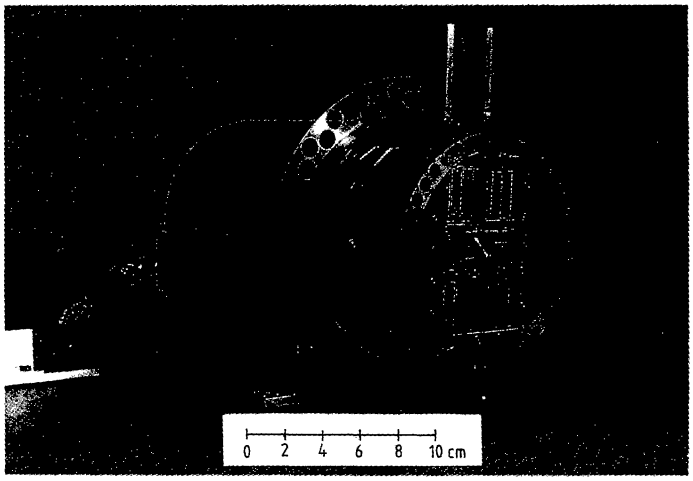

FIGURE 9. The GAS-instrument with thermal-protection blankets removed. The detector system is housed in the rectangular box on the front side. The larger of the two rings with hole patterns (for weight saving) serves for attaching the spacecraft thermal blanket, whereas the smaller one supports the instrument's individual thermal mantle. The instrument section in front of the larger ring is rotatable and protrudes from the spacecraft skin. The optical baffle (pointing upward) was later replaced by an asymmetric one.

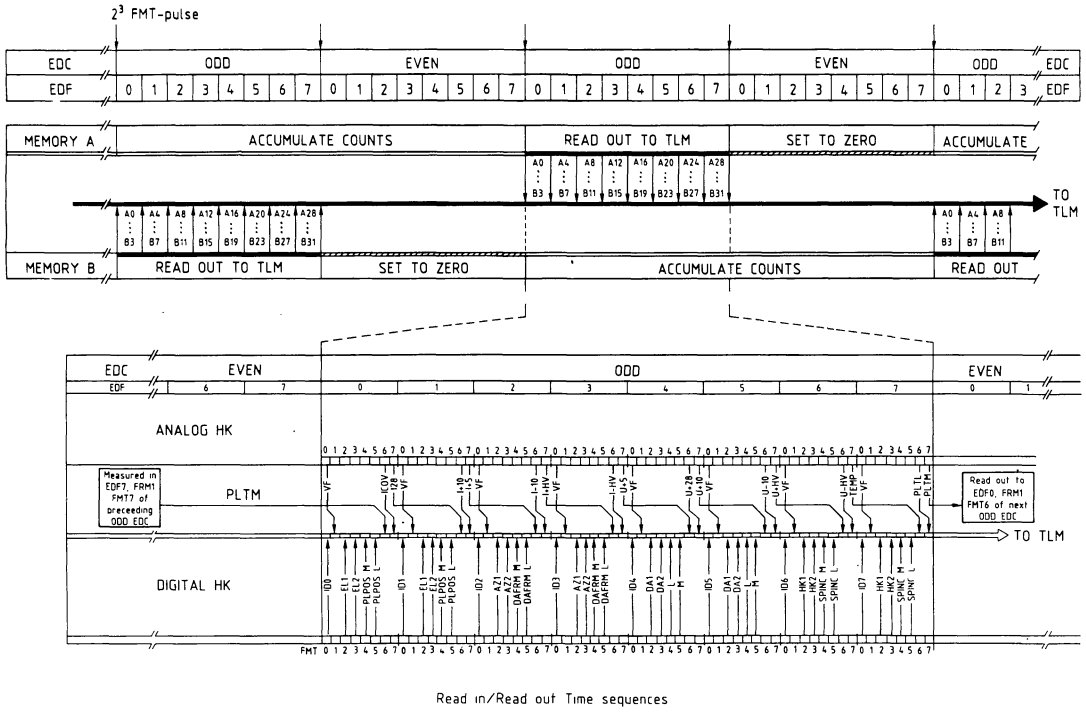

FIGURE 10. The relative timing of the science data (A00...B31), the analogue and digital housekeeping data and their occurrence in the telemetered data stream is shown. Only in the odd experiment data cycles (EDC) data are transmitted. Digital HK-data are transferred immediately to the telemetry (TLM) data stream, analogue HK-data are delayed by one or more telemetry formats (FMT). The science data are accumulated in one of the two memories A or B during one GAS-measurement cycle (GMC = 1 odd + 1 even EDC) and are read out in the next odd EDC. While one memory is read out to telemetry and reset, the other memory is accumulating data. (The abbreviations are explained in Tab. 3).

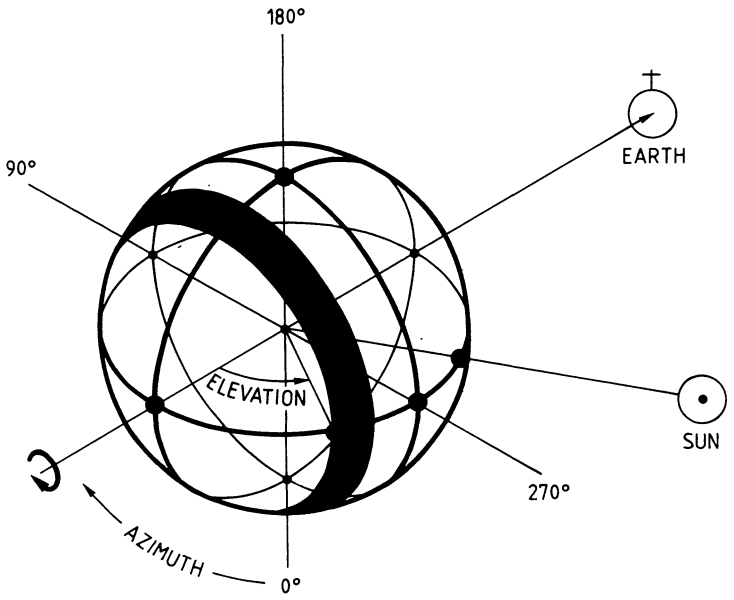

FIGURE 11. The spherical coordinate system of the experiment (azimuth (α) and elevation (ε)), centered in the spacecraft, is oriented always such that the spin axis ($\varepsilon = 180°$) is pointing towards the Earth and the azimuth $\alpha = 270°$ is fixed at the direction towards the Sun. Accordingly, as long as the spacecraft is in the ecliptic plane, at $\alpha = 0°$ (180°) the instrument is pointing to the south (north) pole of the ecliptic plane. At a given elevation angle (ε) the instrument scans along a ring (indicated black), and by varying the elevation the whole celestial sphere can be scanned.

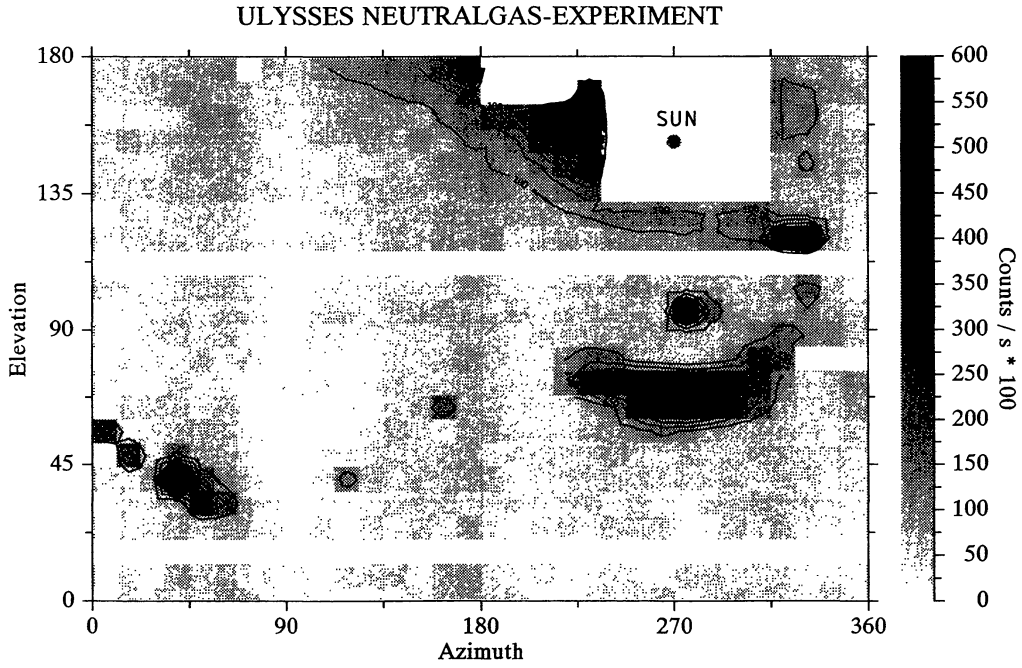

FIGURE 12. One of the first scans of the sky in the "light" of neutral particles. The coordinate system used is a cartesian representation of the spherical system, described in Figure 11. The angular distribution of the neutral particles is clearly visible in the "banana"-like structure ($\alpha \approx 270°$, $\varepsilon \approx 80°$).